

Article

Computational Analysis of Haemodynamic Indices in Synthetic Atherosclerotic Coronary Networks

Sergey Simakov ^{1,2,3,*} , Timur Gamilov ^{1,2,4} , Fuyou Liang ^{4,5}  and Philipp Kopylov ⁴ 

- ¹ Marchuk Institute of Numerical Mathematics, Russian Academy of Sciences, 119991 Moscow, Russia; gamilov@crec.mipt.ru
 - ² Department of Computational Physics, Moscow Institute of Physics and Technology, 141701 Dolgoprudny, Russia
 - ³ Institute of Personalized Medicine, Sechenov University, 119992 Moscow, Russia
 - ⁴ World-Class Research Center “Digital Biodesign and Personalized Healthcare”, Sechenov First Moscow State Medical University, 19991 Moscow, Russia; fuyouliang@sjtu.edu.cn (F.L.); fjk@inbox.ru (P.K.)
 - ⁵ Department of Engineering Mechanics, School of Naval Architecture, Ocean and Civil Engineering, Shanghai Jiao Tong University, Shanghai 200240, China
- * Correspondence: simakov.ss@phystech.edu

Abstract: Haemodynamic indices are widely used in clinical practice when deciding on a particular type of treatment. Low quality of the computed tomography data and tachycardia complicate interpretation of the measured or simulated values. In this work, we present a novel approach for evaluating resistances in terminal coronary arteries. Using 14 measurements from 10 patients, we show that this algorithm retains the accuracy of 1D haemodynamic simulations in less detailed (truncated) geometric models of coronary networks. We also apply the variable systole fraction model to study the effect of elevated heart rate on the values of fractional flow reserve (FFR), coronary flow reserve (CFR) and instantaneous wave-free ratio (iFR). We conclude that tachycardia may produce both overestimation or underestimation of coronary stenosis significance.

Keywords: 1D haemodynamics; stenosis; systole variations; coronary circulation; tachycardia; boundary conditions; FFR; CFR; iFR



Citation: Simakov, S.; Gamilov, T.; Liang, F.; Kopylov, P. Computational Analysis of Haemodynamic Indices in Synthetic Atherosclerotic Coronary Networks. *Mathematics* **2021**, *9*, 2221. <https://doi.org/10.3390/math9182221>

Academic Editor: Jianjun Paul Tian

Received: 31 July 2021

Accepted: 6 September 2021

Published: 10 September 2021

Publisher's Note: MDPI stays neutral with regard to jurisdictional claims in published maps and institutional affiliations.



Copyright: © 2021 by the authors. Licensee MDPI, Basel, Switzerland. This article is an open access article distributed under the terms and conditions of the Creative Commons Attribution (CC BY) license (<https://creativecommons.org/licenses/by/4.0/>).

1. Introduction

Coronary artery disease (CAD) implicates the decrease of blood flow in the heart arteries due to the growth of atherosclerotic plaque. CAD remains one of the leading reasons for disability or death in the world. The severity of the disease dictates a choice between noninvasive treatment (e.g., drug administration) and invasive surgical procedures invoking stent installation. In modern medicine, the decision strongly depends on the analysis of the coefficients characterizing the haemodynamic conditions. Medical doctors widely use fractional flow reserve (FFR), coronary flow reserve (CFR), and instantaneous wave-free ratio (iFR) for evaluating the functional severity of epicardial coronary stenosis [1,2]. The measurement of the haemodynamic indices in clinics requires invasive, expensive procedures with possible side effects.

Computational simulations based on noninvasive data become an excellent alternative [3,4]. Coronary hemodynamics simulation is a well-developed field with numerous contributions [5–8]. Virtual modelling tool model for FFR assessment managed to get an FDA (U.S. Food and Drug Administration) approval [8]. It is based on 3D hemodynamics in coronary arteries. 3D models are well-suited for simulations of blood flow in atherosclerotic areas with complex geometry. Patient-specific geometry of coronary arteries can be extracted from coronary computed tomography angiography (CCTA) images. 1D models of coronary circulation can be used as an alternative to demanding 3D computations. It was demonstrated that 1D estimation of FFR could have accuracy similar to the 3D approach [9,10]. The works [3,11] present 1D mathematical models for FFR evaluation.

The iFR simulations are addressed in [12,13]. The computations of CFR are performed in [14,15]. The work [16] presents a benchmark comparison of four numerical approaches with clinical data on FFR. All approaches demonstrate good performance, although they depend on the uncertainty of the input medical images.

Essential factors for correct clinical interpretation and decision making are the accuracy and sensitivity of the mathematical model to the quality of the input data and diagnostic implications of various coefficients. These aspects were partly studied in [14,17,18]. e.g., ventricular pacing and tachycardia may potentially disturb coronary haemodynamics and change the values of FFR, CFR and iFR. Properly developed CCTA imaging protocols can significantly improve results of FFR estimation with mathematical models [19]. The introduction of numerical approaches into clinical practice means that FFR estimation technology will have to be implemented in various clinical centers with different CCTA imaging protocols and computed tomography (CT) scan machines. The low quality of CT data makes small coronary arteries unrecognizable for segmentation algorithms. It leads to decreased geometric details of the coronary network and may affect calculated values of FFR, CFR and iFR.

In this work, we consider two important issues of the numerical evaluation of FFR, CFR and iFR by 1D haemodynamic model of coronary flow. The first is the sensitivity of simulations to the quality of CT data. The second is the effect of the heart rate on the FFR, CFR and iFR variability. In Section 2.1 we briefly present a 1D haemodynamic model of coronary flow. We extend it with the model of variable stroke volume (SV) and length of the systole depending on a heart rate (HR). This model was previously applied to the analysis of average coronary blood flow (CBF) during asynchronous pacing and arrhythmias [20]. The input and modified patient data are described in Section 2.2. We assume that low-quality CT data contain less information on smaller vessels in the coronary network and remove most of them. Section 2.3 presents a novel recursive algorithm of the peripheral resistance distribution from the aortic root to distal vessels based on Murray's law at every level. This algorithm is applied both to the input and reduced networks. Section 2.4 contains definitions of haemodynamic indices (FFR, CFR, iFR) used in this work. In Section 3.1 we compare haemodynamic indices in the input and reduced networks. In Section 3.2 we study the effect of HR elevation on the FFR, CFR and iFR. The results are discussed in Section 4.

We conclude that the new algorithm of peripheral resistance distribution throughout a network makes the mathematical model almost insensitive to the absence of the smallest arteries. It produces less or similar error than the distribution algorithm among terminal vessels regardless of the parent's vessels. It also does not require information on the patient's coronary dominance type, unlike other approaches [16]. We also conclude that tachycardia can lead to overestimating or underestimating stenosis significance due to the complex relationship between haemodynamic indices and heart rate.

2. Materials and Methods

2.1. 1D Mathematical Model of the Blood Flow in the Network of Coronary Vessels

The blood flow in the coronary vascular network and the aorta is simulated by a 1D reduced-order model of unsteady flow of viscous incompressible fluid through the network of elastic tubes. The details of this approach can be found in [21,22]. The 1D models were adapted and applied to the coronary circulation in [20,23]. In this section we present a brief description of 1D model. The flow in every vessel is described by mass and momentum balances

$$\frac{\partial \mathbf{V}}{\partial t} + \frac{\partial \mathbf{F}(\mathbf{V})}{\partial x} = \mathbf{G}(\mathbf{V}), \quad (1)$$

$$\mathbf{v} = \begin{pmatrix} A \\ u \end{pmatrix}, \mathbf{F}(\mathbf{V}) = \begin{pmatrix} Au \\ u^2/2 + p(A)/\rho \end{pmatrix}, \mathbf{G}(\mathbf{V}) = \begin{pmatrix} 0 \\ \psi \end{pmatrix},$$

where t is the time, x is the distance along the vessel counted from the vessel's junction point, ρ is the blood density (constant), $A(t, x)$ is the vessel cross-section area, p is the blood pressure, $u(t, x)$ is the linear velocity averaged over the cross-section, ψ is the friction force

$$\psi = -8\pi\mu \frac{u}{A}, \tag{2}$$

μ is the dynamic viscosity of the blood. The relationship between pressure and cross-section is defined by wall-state equation:

$$p(A) = \rho_w c^2 F(A), \tag{3}$$

where ρ_w is vessel wall density (constant), c is the velocity of small disturbances propagation in the material of the vessel wall, $F(A)$ is monotone S-like function (see [21] for a review)

$$F(A) = \begin{cases} \exp(\eta - 1) - 1, & \eta > 1 \\ \ln \eta, & \eta \leq 1 \end{cases}, \eta = \frac{A}{\tilde{A}}, \tag{4}$$

where \tilde{A} is the cross-sectional area of the unstressed vessel.

At the vessel's junction points we impose mass conservation condition and continuity of the total pressure:

$$\sum_{k=k_1, k_2, \dots, k_M} \varepsilon_k A_k(t, \tilde{x}_k) u_k(t, \tilde{x}_k) = 0, \tag{5}$$

$$p_k(A_k(t, \tilde{x}_k)) + \frac{\rho u^2(t, \tilde{x}_k)}{2} = p_{k+1}(A_{k+1}(t, \tilde{x}_{k+1})) + \frac{\rho u^2(t, \tilde{x}_{k+1})}{2}, k = k_1, k_2, \dots, k_{M-1}, \tag{6}$$

where k is the index of the vessel, M is the number of the connected vessels, $\{k_1, \dots, k_M\}$ is the range of the indices of the connected vessels, $\varepsilon = 1, \tilde{x}_k = L_k$ for incoming vessels, $\varepsilon = -1, \tilde{x}_k = 0$ for outgoing vessels.

The boundary conditions at the aortic root include the blood flow from the heart, which is set as a predefined time function $Q_H(t)$

$$u(t, 0)A(t, 0) = Q_H(t). \tag{7}$$

In this work, we use a simple approximation of the heart outflow $Q_H(t)$ in the time domain. We define it as a half-sine function during ventricular systole and set it to zero otherwise

$$Q_H(t) = \begin{cases} SV \frac{\pi}{2\tau} \sin\left(\frac{\pi t}{\tau}\right), & 0 \leq t \leq \tau, \\ 0, & \tau < t \leq T, \end{cases} \tag{8}$$

where SV is the stroke volume of the left ventricle, T is the period of the cardiac cycle, τ is the duration of the systole. Thus, the stroke volume is

$$SV = \int_0^T Q_H(t) dt \tag{9}$$

and cardiac output (CO) by definition [24] equals

$$Q_{CO} = SV \cdot HR. \tag{10}$$

The dependency of τ from HR is nonlinear. Previously we derived the function $\tau(T)$ as a regression basing on the results of simulations of action potential dynamics in human cardiac cells with the O'Hara-Rudy model [20]

$$\tau = 287.09[\text{ms}] - \frac{30685.24[\text{ms}^2]}{T[\text{ms}]}. \tag{11}$$

Experimental and clinical studies [25,26] report a linear relationship between SV and HR . Thus, we use linear regression obtained in [20]

$$SV = SV_0[\text{ml}] - \frac{HR[\text{bpm}]}{\alpha}. \tag{12}$$

We adjust SV_0 according to the patient’s data on HR and SV . According to clinical studies [25,26] $\alpha = 2[\text{bpm/mL}]$ and this value vary only slightly among patients. Finally, we use (11) and (12) for parametrization of $Q_H(t)$ in (8) for various heart rates.

The outflow boundary conditions assume that a terminal artery with index k is connected to the venous pressure reservoir with the pressure $p_{veins} = 8 \text{ mmHg}$ through a hydraulic resistance R_k . It is described by Poiseuille pressure drop condition

$$p_k A_k - p_{veins} = R_k A_k u_k, \tag{13}$$

where p_k, A_k, u_k are blood pressure, cross-sectional area and blood velocity at the terminal point of k -th vessel. We use the same outflow condition for the aorta and coronary arteries.

The hyperbolic system (1) inside every vessel is numerically solved by the grid-characteristic method of the second order [27]. The systems of nonlinear algebraic equations in vessel’s junctions (5) and (6), aortic root (7) and at the end points of terminal arteries (13) are numerically solved by the Newton’s method. To close the system of nonlinear equations, we add the mass conservation condition and second-order compatibility conditions of hyperbolic set (1).

Compatibility conditions can be derived from the characteristic form of hyperbolic system (1):

$$\omega_i \cdot (\partial \mathbf{V} / \partial t + \partial \mathbf{F} / \partial x) = \omega_i \cdot (\partial \mathbf{V} / \partial t + \lambda_i \partial \mathbf{V} / \partial x) = \omega_i \cdot \mathbf{G}, \quad i = 1, 2 \tag{14}$$

where λ_i are the eigenvalues of the Jacobi matrix $\mathbf{A} = \partial \mathbf{F} / \partial \mathbf{V}$; ω_i are the eigenvectors of the \mathbf{A} .

We use Equation (14) with positive λ_i for the vessel’s terminal point ($\tilde{x} = L$) and negative λ_i for its initial point ($\tilde{x} = 0$). After implicit finite difference discretization we obtain linear relation between $u(t_{n+1}, \tilde{x})$ and cross section area $A(t_{n+1}, \tilde{x})$:

$$u(t_{n+1}, \tilde{x}) = \alpha A(t_{n+1}, \tilde{x}) + \beta, \tag{15}$$

where \tilde{x} is a boundary coordinate. Coefficients α and β depend on a type of discretization (order, stencil) as well as values of $\lambda_i, \mathbf{V}, \omega_i$. In this work we use second order implicit discretization.

The computational domain is the network of vessels, including the aortic root, aorta, left and right coronary arteries and their branches. The aorta and other systemic arteries are simulated as a single vessel with the length set to 80 cm and diameter set to 2.17 cm. We refer to this vessel as the ‘aorta’ since most of its properties correspond to the patient’s aorta (diameter, elasticity). The aorta’s parameters are adjusted to represent compliance of a systemic circle and to get an adequate arteriovenous pressure drop (see Section 2.3). On the inflow of the aortic root, we set boundary condition (7). The aortic root splits into three branches: aorta, left coronary artery (LCA) and right coronary artery (RCA). The sum of average blood flow through LCA and RCA is a coronary blood flow (Q_{cor} in Section 2.3). The geometrical properties of the aortic root and coronary arteries are extracted from patients’ CT scans.

2.2. Patient Data

We investigated a cohort of 10 patients with 14 sites of FFR measurements. Patients’ data are freely available and presented in detail in [16]. The data included 3D surface meshes, 1D meshes, patient clinical data with measured FFR and calculated FFR values, and sketches from clinicians indicating the approximate location of FFR measurement. Patient

clinical data included blood pressure measurements (systolic, diastolic and average), body mass index (BMI), age, heart rate during CT acquisition. Table 1 briefly summarizes clinical data used in this work.

We used the patient's age to estimate pulse wave velocity [28] that equals to the velocity of small disturbances propagation c in (3). Stroke volume was estimated based on BMI values according to [29]. We used blood pressure measurements to estimate resistance for aortic outflow boundary condition (13). Resistances for terminal coronary arteries were set according to a recursive algorithm (see Section 2.3).

Table 1. Clinical data for patients. Stroke volume values are estimated based on patient's BMI. CD—coronary dominance.

Patient	Average Pressure, mmHg	SV, ml	HR, bpm	CD Type	Stenosis Site	FFR
1	111	82	67	Left	LAD	0.89
2	83	82	80	Right	LAD	0.86
3	125	65	72	Right	RCA	0.88
4	94	70	88	Left	LAD	0.82
5	99	82	73	Left	LAD	0.82
6	99	70	48	Right	LAD proximal LAD distal DA	0.9 0.82 0.81
7	98	82	48	Right	LAD LCX	0.75 0.84
8	110	70	85	Right	LAD LCX	0.88 0.89
9	90	70	75	Right	LAD	0.83
10	108	68	58	Right	LAD	0.72

Patient-specific geometries were obtained from the CT images by the method of automatic CT scans processing [21]. We refer to these geometries as 'full' coronary trees. The method included four stages: aorta segmentation; computation of Frangi vesselness; ostia point detection and coronary artery segmentation; skeletonization of segmented arteries, and graph construction.

In this work, we investigated the sensitivity of haemodynamic indices to the degree of coronary network details. We synthetically generated 'reduced' low-detailed coronary trees by cutting full trees. We removed all branches distal to the location of FFR measurement (provided there were no other sites of FFR measurements downstream). All junctions proximal to the location of the FFR-measurement were preserved to ensure adequate flow distribution. All junctions without distal FFR-measurement sites were removed. An example is shown in Figure 1.

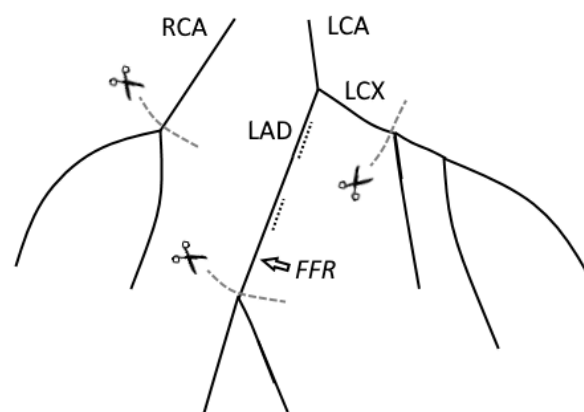


Figure 1. Cutting branches of full trees to generate reduced trees for Patient 1. Dotted lines designate stenoses. We preserve arteries and junctions proximal to FFR-measurement sites while removing the rest.

Reduced trees represent synthetically generated coronary trees with low segmentation quality. We cut full trees as much as possible without affecting the FFR-measurement site. This cutting algorithm could also save computational time, provided it did not significantly affect the values of haemodynamic indices.

2.3. Terminal Resistance

Myocardium compression is an essential feature of coronary haemodynamics. We simulated compressions by setting $R_k = R_k(t)$ for the boundary condition (13) in the terminal coronary arteries. Similar to our previous works [20] we assumed that the shape of $R_k(t)$ was the same as the time profile of a cardiac output (8).

$$R_k(t) = \begin{cases} R_k + (R_k^{max} - R_k) \sin\left(\frac{\pi t}{\tau}\right), & 0 \leq t \leq \tau, \\ R_k, & \tau < t \leq T. \end{cases} \tag{16}$$

The peak value of the terminal resistance during systole was set to $R_k^{max} = 3R_k$, where R_k is the terminal resistance during diastole [16]. It was sufficient for the complete blockage of the flow in terminal CAs during systole.

The values of R_k were set according to the following algorithm. First, we estimated the outflow resistance of an aortic part (R_a) and the total effective resistance of a coronary part (R_{cor}). Aortic resistance was prescribed at the end of the virtual vessel representing aorta and systemic circulation. We assume that R_a produces the pressure drop $\Delta P = P_{ave} - p_{veins}$ mmHg, where $p_{veins} = 8$ mmHg is venous pressure [24], P_{ave} is measured average blood pressure in systemic circulation. We also assume that the ratio of coronary blood flow (CBF) to minute cardiac output (CO) is $\beta = 0.05$ ($Q_{cor} = \beta Q_{CO}$). Thus we have

$$R_a = \frac{\Delta P}{(1 - \beta) \cdot Q_{CO}}, \quad R_{cor} = \frac{\Delta P}{\beta Q_{CO}}, \tag{17}$$

where R_{cor} is total resistance of coronary microcirculation and Q_{cor} is average coronary blood flow (CBF). As a result, we have $R_{cor} = 19R_a$. In our simulations, these values produced the calculated ratio of β between 0.03 and 0.06, which belong to the well known physiological range [24,30,31]. The value of β varied depending on the particular resistance of an arterial network.

Second, we assigned terminal resistances R_k for each terminal coronary artery. We proposed a recursive algorithm that splits resistances in each branching point according to Murray’s law with a power of 2.27 [32]. Let us consider parent branch and N child branches with diameters $d_i, i = 1, 2, \dots, N$ (Figure 2). The parent branch supplies a region of the myocardium with resistance R . The child branch with index i supplies a subregion with resistance R_i . Our goal was to calculate resistances $R_i, i = 1, 2, \dots, N$.

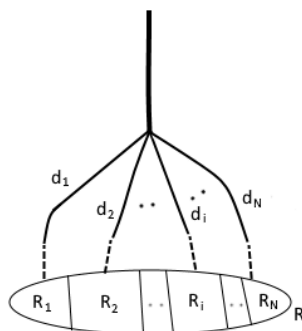


Figure 2. Resistance distribution from parent branch to child branches.

We assume that

$$\frac{1}{R} = \sum_{i=1}^N \frac{1}{R_i}, \quad R_i \propto \frac{1}{Q_i} \propto \frac{1}{d_i^p}, \tag{18}$$

where $p = 2.27$ and Q_i is an average blood flow through i -th child branch. Using (18) we derive R_i as a function of R_1

$$R_i = R_1 \left(\frac{d_1}{d_i} \right)^p, \quad i = 1, 2, \dots, N. \tag{19}$$

Finally, from (18) and (19) we get

$$R_1 = R \sum_{i=1}^N \left(\frac{d_i}{d_1} \right)^p. \tag{20}$$

We used expressions (19) and (20) to calculate $R_i, i = 1, 2, \dots, N$. The recursive algorithm starts by applying procedure (19), (20) to the roots of LCA and RCA. We consider R_{cor} as a parent branch resistance (R in (20)) and LCA and RCA as two child branches ($N = 2$). We calculated resistances corresponding to LCA and RCA roots. After that, we treated LCA and RCA as parent branches and traverse all coronary networks with the depth-first search until we calculated resistance R_k for each terminal artery. We will refer to this algorithm as a ‘recursive algorithm’ or option A.

A general method to distribute terminal resistances involves dividing R_{cor} directly between terminal points of an arterial network, ignoring diameters of all branches in between. We will refer to this approach as the ‘terminal points algorithm’ or option B. This approach is typically modified to consider coronary dominance type [16] or arterial network resistance [33]. Our calculations used a basic version of the ‘terminal points algorithm’ since most of the modifications could be improved by implementing a recursive version.

2.4. Haemodynamic Indices

We simulated stenosis as a separate part of the vessel with reduced diameter and increased velocity of small disturbances propagation c (3) (by a factor of 2). We performed two calculations for stenosed trees—under normal conditions and with vasodilatation (hyperemia). Vasodilatation was simulated with the same model with reduced terminal resistances R_k of coronary arteries for the boundary condition (13). We reduced resistances by 70% [16,34].

Fractional flow reserve (FFR) was calculated as the ratio of average pressure in coronary artery distal to stenosis (\bar{P}_{dist}^h) to average aortic pressure (\bar{P}_{aortic}^h) during hyperemia.

$$FFR = \frac{\bar{P}_{dist}^h}{\bar{P}_{aortic}^h}. \tag{21}$$

Values of $FFR < 0.8$ typically correspond to hemodynamically significant lesions.

Coronary flow reserve (CFR) was calculated as the ratio of average blood flow through stenosed vessel during hyperemia (\bar{Q}^h) to average blood flow through stenosed vessel under nonhyperemic normal condition (\bar{Q}^n).

$$CFR = \frac{\bar{Q}^h}{\bar{Q}^n}. \tag{22}$$

Values of $CFR < 2.0$ typically correspond to hemodynamically significant lesions.

Instantaneous wave-free ratio (iFR) is defined as the ratio between average pressure in coronary artery distal to stenosis (\bar{P}_{dist}^w) and average aortic blood pressure (\bar{P}_{aortic}^w) during

the diastolic wave-free period (WFP) under the nonhyperemic normal condition. WFP begins 25% of the way into diastole and ends 5 ms before the end of diastole [35].

$$iFR = \frac{\overline{P}_{dist}^w}{\overline{P}_{aortic}^w}. \quad (23)$$

The borderline value of iFR is 0.9. Values below 0.9 are associated with severe CAD.

3. Results

3.1. Haemodynamic Indices Sensitivity to Coronary Tree Detailization

In this section, we present the results of calculating haemodynamic indices for two resistance distribution algorithms: recursive algorithm and terminal points algorithm (see Section 2.3). We compare the computed values for the cases of full trees and reduced trees.

We started with evaluating blood flow distribution between coronary arteries. We wanted to demonstrate that the recursive algorithm provided proper distribution of CBF between LCA and RCA without any additional data on coronary dominance type. Figure 3 shows CBF distribution between LCA and RCA calculated with the recursive algorithm on full coronary trees. Patients 1, 4 and 5 had the highest ratio of blood flow in LCA to blood flow in RCA. These patients were marked as left-dominant type by a cardiologist. The rest of the patients were marked as right-dominant type. The mean value of LCA blood flow proportion was 79.6% among left-dominant patients (patients 1, 4, 5) and 58.5% among right-dominant patients (patients 2, 3, 6–10). These values were in good agreement with clinical data [30]: 76.1% and 57.8%, respectively. We concluded that the recursive algorithm automatically considered coronary dominance type and distributes blood flows accordingly. It reduced the need for cardiologist expertise during cardiovascular simulations.

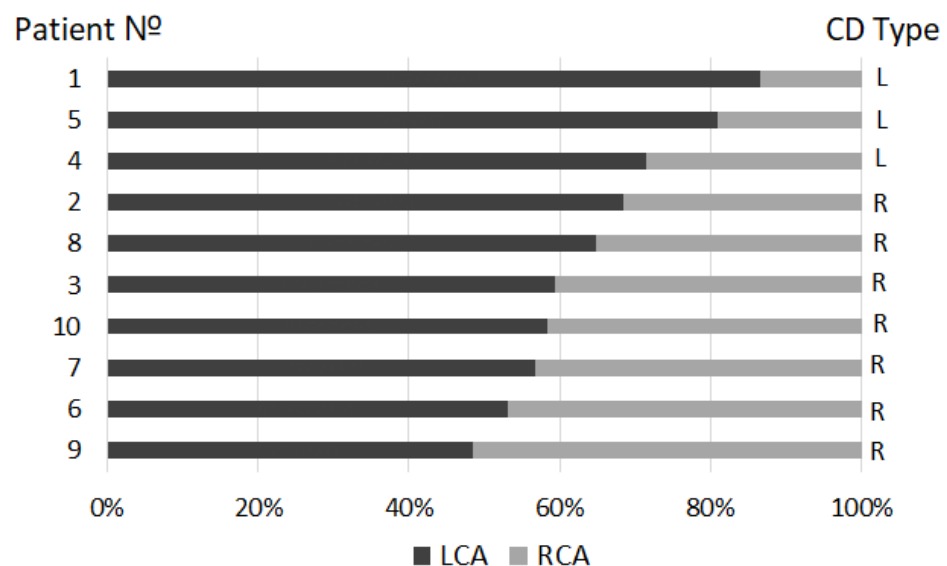


Figure 3. The fraction of CBF in LCA and RCA for all patients, which was calculated for full trees by the recursive algorithm under nonhyperemic (normal) conditions. CD—coronary dominance: R—right dominant type, L—left dominant type. Patients (on the left) are arranged from the largest to the smallest proportion of LCA blood flow. For exact values see Table A1.

To investigate the effect of coronary tree details on CBF distribution, we compared LCA and RCA blood flows for full trees and reduced trees (see Section 2.2). The average difference in blood flow through LCA between full trees and reduced trees for the recursive algorithm was 4%. For RCA, the average difference was 3%. For the terminal point algorithm of resistances distribution, the average difference in blood flow through LCA

between full trees and reduced trees was 10%. For RCA, the average difference was 18%. It demonstrated that the terminal points algorithm was quite sensitive to the degree of details of an arterial tree. This algorithm may produce significant errors when calculating haemodynamic indices, since small coronary arteries could be easily missed due to poor CT data quality. On the other hand, the recursive algorithm was less sensitive to coronary tree detalization (4% error for LCA, 3% error for RCA). The recursive algorithm allowed for more significant errors during CT acquisition and segmentation.

Next, we investigated the effect of coronary tree details on haemodynamic indices. We compared sensitivity to the degree of tree details in two resistance distribution algorithms: recursive algorithm and terminal points algorithm. FFR, CFR and iFR values for full trees were taken as the base values. We calculated haemodynamic indices for reduced trees and presented root-mean-square error (RMSE) relative to the base values. We also presented normalized RMSE (NRMSE) as a ratio between RMSE and the mean base index value (sum of all indices divided by the number of the stenoses).

Table 2 shows mean calculated values of haemodynamic indices, RMSE and NRMSE values between indices, which were calculated for the full trees and reduced trees by the recursive and terminal points algorithms. NRMSEs of FFR, CFR and iFR were 1–2% for the recursive algorithm and 5–7% for the terminal points algorithm. It meant that haemodynamic indices were less sensitive to the detalization of the coronary tree in the case of the recursive algorithm.

Table 2. Sensitivity of FFR, CFR, iFR to coronary tree detalization for two cases: (1) resistances distributed with recursive algorithm, (2) resistances distributed with terminal points algorithm. RMSE—root-mean-square error, NRMSE—normalized root-mean-square error. RMSE and NRMSE are calculated between indices (FFR, CFR, iFR) calculated on full trees and reduced trees.

Algorithm (Section 2.3)	FFR		CFR		iFR	
	Recursive	Terminal	Recursive	Terminal	Recursive	Terminal
Mean value (full trees)	0.85	0.82	2.46	2.40	0.93	0.91
RMSE	0.008	0.05	0.05	0.17	0.01	0.05
NRMSE	1%	6%	2%	7%	1%	5%

Figures 4–6 present the detailed analysis of the difference between the FFRs, CFRs and iFRs, which were calculated for the full trees and reduced trees by the recursive and terminal points algorithms. We observed that the recursive algorithm produced substantially less divergence in all cases. The terminal points algorithm demonstrated acceptable performance in the upper parts of the range, but it failed in the lower parts. The most significant deviations were observed in the case of patient 1 for the terminal points algorithm. The distribution of flows between LCA and RCA for this patient changed significantly after cutting the full tree. Change in LCA blood flow for patient 1 equaled 22% (most significant among all patients), which caused substantial deviations in the calculated indices.

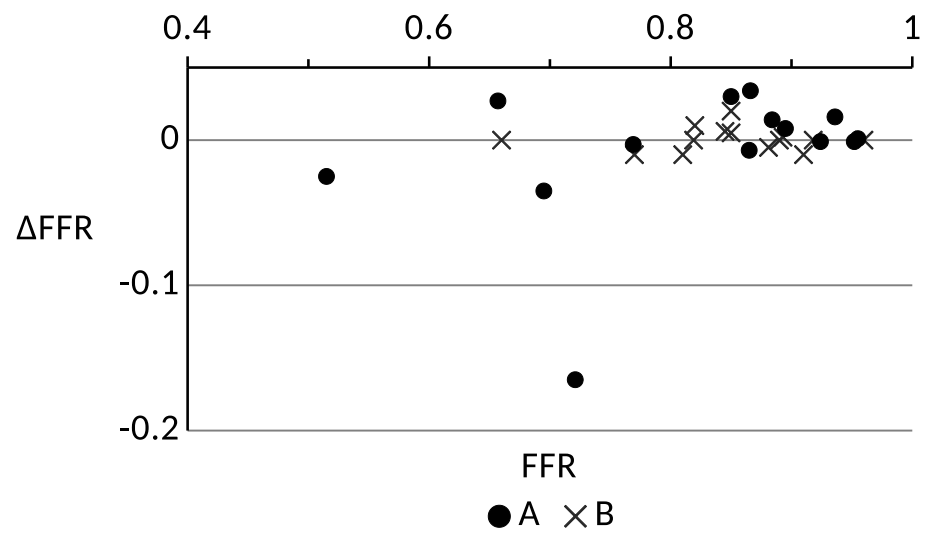


Figure 4. Difference between the FFRs, which were calculated for the full trees and reduced trees (A—recursive algorithm, B—terminal points algorithm).

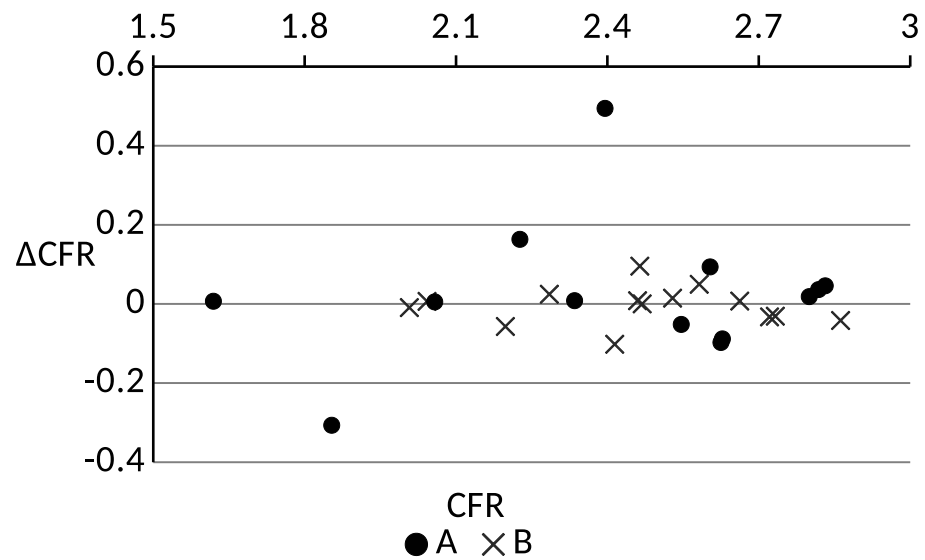


Figure 5. Difference between the CFRs, which were calculated for the full trees and reduced trees (A—terminal points algorithm, B—recursive algorithm).

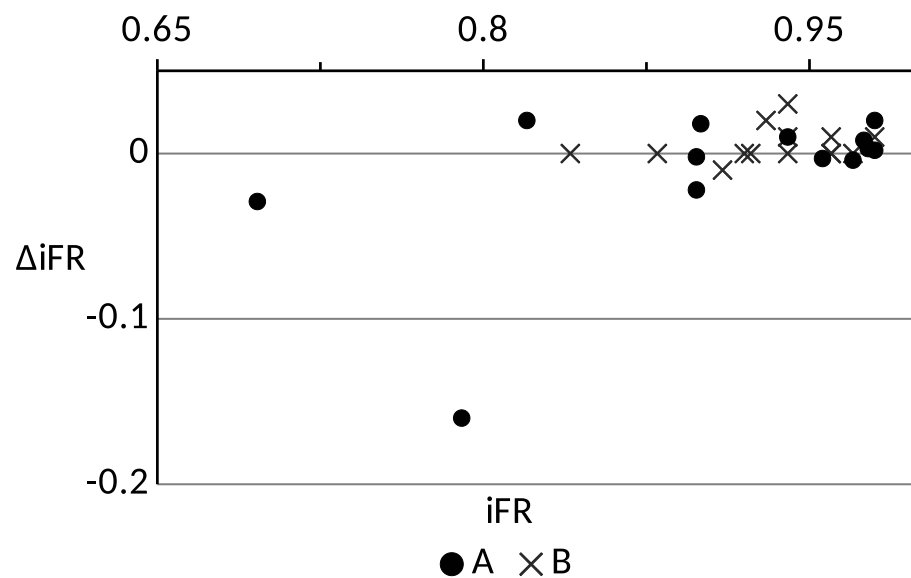


Figure 6. Difference between the iFRs, which were calculated for the full trees and reduced trees (A—terminal points algorithm, B—recursive algorithm).

3.2. Haemodynamic Indices Sensitivity to Heart Rate

In this section, we calculated FFR, CFR and iFR for various heart rates from 60 bpm to 120 bpm. All presented results corresponded to the full trees and recursive algorithm of resistances distribution. First, we validated our model by calculating FFR values for baseline values of HR and SV (see Table 1). Results are presented in Figure 7. RMSE between calculated and measured FFR was 0.04 or 5%, with sensitivity and specificity equal to 1.0. Thus, we reported adequate performance of the computational algorithm.

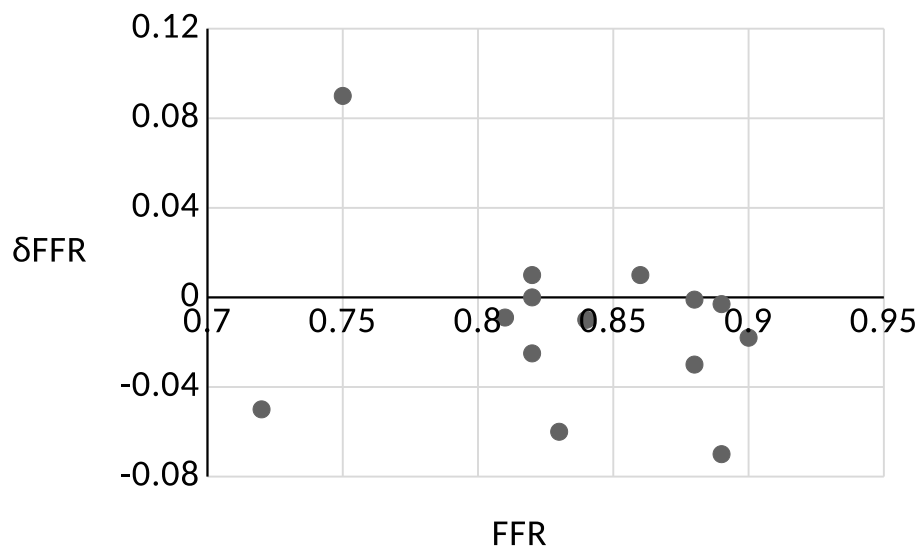


Figure 7. Difference between the FFRs, which were calculated for the full trees by the recursive algorithm, and measured FFRs.

Next, we investigated the sensitivity of haemodynamic indices to heart rate. We adjusted stroke volume (12) and systolic duration (11) for each value of heart rate.

Figures 8–10 demonstrate sensitivity of haemodynamic indices to heart rate. Exact values are presented in Tables A2–A4. In our previous works [36] we concluded that FFR decreased with an increase of HR or SV. It meant that the haemodynamic significance of stenosis increased with cardiac output. However, in this work, we considered the relation between HR, SV and systolic duration. In most cases in the Figures 8–10, haemodynamic

indices did not change significantly within 60–120 bpm range. In some cases an index decreased initially and then increased (see FFR, patient 7, left anterior descending artery—LAD, Table A2). In other cases an index steadily decreased (see FFR value of patient 4, Table A2) or increased (see CFR value of patient 7, circumflex artery—LCX, Table A3). We concluded that the relation between haemodynamic indices and heart rate included a lot of other parameters which were not addressed in this work. Indices may have increased or decreased, but in most cases, they did not change significantly.

We assumed that FFR, CFR and iFR behaviour depended on various factors: stenosis degree, artery diameter, patient’s cardiac output, etc. Additional studies should be performed on an extended cohort of patients to investigate these factors further. Clinical studies [37] also show that the impact of the HR on haemodynamic indices can vary and depends on the artery and lesion properties.

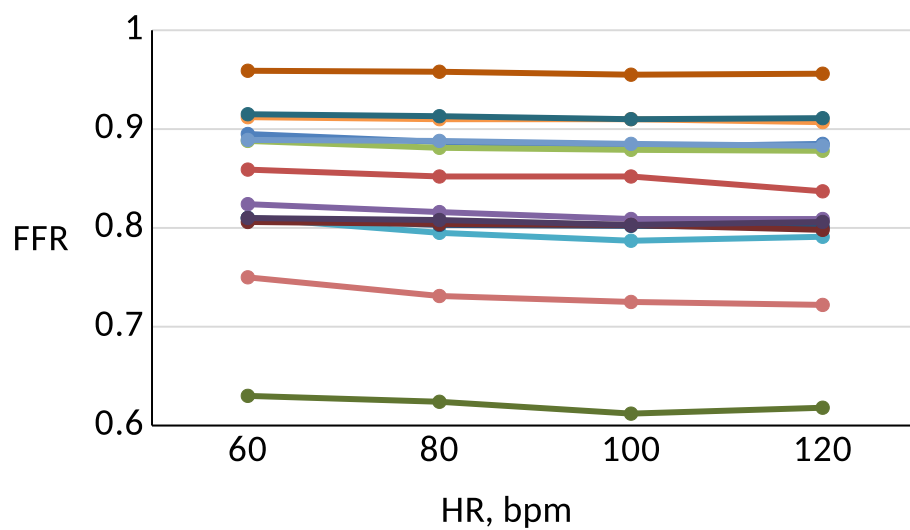


Figure 8. FFR for various heart rates, which was calculated for the full trees by the recursive algorithm.

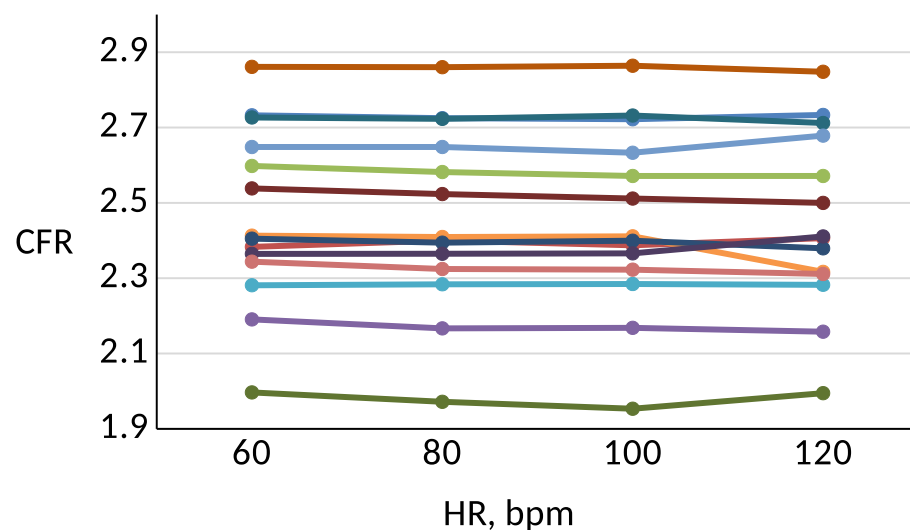


Figure 9. CFR for various heart rates, which was calculated for the full trees by the recursive algorithm.

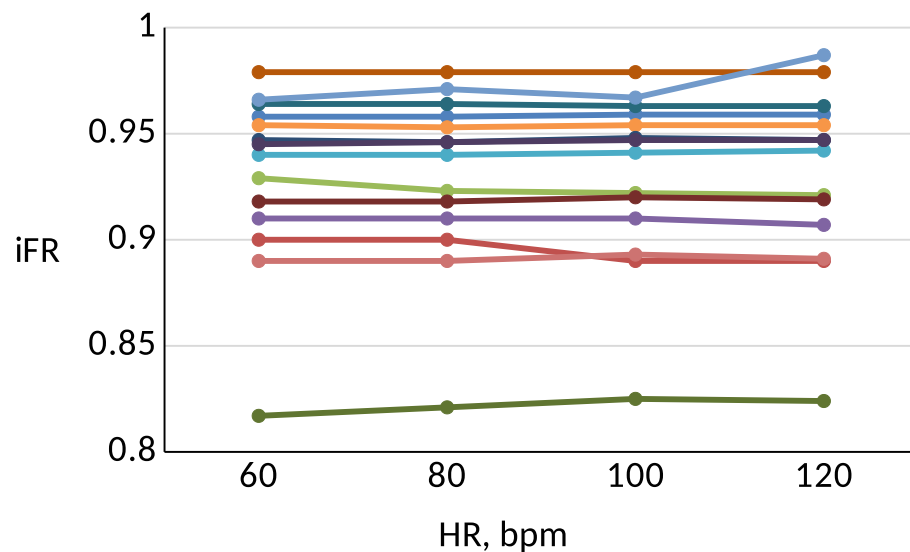


Figure 10. iFR for various heart rates, which was calculated for the full trees by the recursive algorithm.

4. Discussion

This work studied the sensitivity of calculated haemodynamic indices to the degree of coronary tree and heart rate details. We presented a new recursive algorithm of terminal resistances distribution. This algorithm significantly reduces the model's sensitivity to the degree of details of a coronary tree. It needs no preliminary information on a coronary dominance type. In other works, this problem is partially solved by introducing additional coefficients [33], changing algorithm based on the coronary dominance type [16] or performing preliminary calculations [38]. Changing the algorithm based on the coronary dominance type [16] requires additional information from an expert cardiologist. This data may not be available in an actual situation. It also usually considers two coronary dominance types (left and right) and ignores intermediate cases. All these approaches [16,33,38] are valid and effective, but most of them can be further improved by implementing the recursive algorithm. Decreased sensitivity to the details of an arterial tree means that calculated haemodynamic indices are less susceptible to low-quality CT images. It also means that we can synthetically reduce details of an arterial network to reduce calculation time without significant error.

We note that the quality of CT images is essential for accurate FFR, CFR and iFR estimation. We used a specific algorithm for reduced trees generation. We only cut parts of the arterial tree that were not close to FFR measurement sites. Low-quality CT images may result in a missed junction proximal to FFR measurement sites or yield the wrong diameter of the stenosed vessel. In that case, the recursive algorithm may produce a significant error.

Heart rate is an essential factor of coronary haemodynamics [39], but the literature examining its influence on FFR, CFR and iFR is sparse. Results of our study imply that tachycardia might be responsible for an overestimation or underestimation of haemodynamic indices. We did not find a clear pattern to describe a relation between HR and haemodynamic indices. Blood flow in the LAD occurs mainly during diastole and drops to zero (or is even reversed) during systole. However, systolic reduction of blood flow in the RCA is much less evident due to lower right ventricular pressure. It means that changes in systolic duration due to increased HR have a different effect on various arteries. iFR is measured during the diastolic wave-free period. Relative diastole duration shortens significantly at high heart rates, leaving less time for blood flow. As a result, iFR behaviour with increased HR can be different from FFR or CFR. We hypothesize that increased haemodynamic indices at higher heart rates can be attributed to decreased cardiac output during significant tachycardia. Lower values of blood flow tend to decrease the haemodynamic significance of a stenosis.

1D haemodynamics models derived on the basis of various assumptions, which include arguable postulates: the shape of the spatial profile of the velocity is considered static in a cross-section of a vessel; the pressure is described by a predefined function from the cross-section area, etc [21]. Nevertheless, a lot of works demonstrate acceptable accuracy basing on the comparison with clinical data [18,31,33], in vitro experiments on a network of collapsible tubes [40] and 3D simulations [9,10,41]. The periodic contractions of the myocardium cause a periodic collapse of the peripheral haemodynamics. It partially neglects the influence of unrealistic assumptions and allows computing haemodynamic indices with acceptable accuracy basing on the patient-specific datasets [3,4,11–15] and many others. In this work, we use 1D approach with a fairly simple model of stenosis, which fails to simulate blood flow patterns near calcified plaques with complex geometry. It means that calculated FFR values can be underestimated in some cases. Our approach relies on expert's assessment of stenosis degree that introduces additional human error.

Lack of CFR and iFR measurements (as well as measurements of FFR for various heart rates) constrains our study. We assumed similar relation between SV and HR for all patients. This approach may produce increased error in FFR, CFR, iFR estimations at higher heart rates. Some further studies should include measurements of haemodynamic indices or at least measurements of stroke volume and systolic duration for various heart rates. The latter could identify the relation between SV, systolic duration and HR for each patient and improve our estimate of tachycardia effect on coronary circulation. These potential results can substantially affect clinical practice, especially regarding clinical decision-making when FFR, CFR, and iFR values are borderline.

Author Contributions: Conceptualization, S.S., P.K.; methodology, S.S., T.G., P.K., F.L.; software, S.S., T.G.; validation, S.S., T.G., F.L.; formal analysis, S.S., T.G., P.K.; writing—original draft preparation, S.S., T.G.; writing—review and editing, S.S., T.G., F.L.; visualization, T.G., S.S.; supervision, S.S., P.K. All authors have read and agreed to the published version of the manuscript.

Funding: This research was funded by Russian Science Foundation grant number 21-71-30023.

Institutional Review Board Statement: Not applicable.

Informed Consent Statement: Not applicable.

Data Availability Statement: Not applicable.

Conflicts of Interest: The authors declare no conflict of interest.

Abbreviations

The following abbreviations are used in this manuscript:

BMI	Body-mass index
bpm	Beats per minute
CA	Coronary arteries
CAD	Coronary artery disease
CBF	Coronary blood flow
CO	Cardiac output
CT	Computed tomography
CCTA	Coronary computed tomography angiography
HR	Heart rate
LAD	Left anterior descending artery
LADd	distal part of LAD
LADp	proximal part of LAD
LCA	Left coronary artery
LCX	Circumflex artery
RCA	Right coronary artery
SV	Stroke volume

Appendix A

Table A1. Calculated average blood flow through LCA and RCA under nonhyperemic conditions for full trees. Resistances are distributed according to recursive algorithm.

	1	2	3	4	5	6	7	8	9	10
LCA, ml/s	2.73	2.58	1.59	2.44	2.45	1.04	1.27	2.33	1.50	1.31
RCA, ml/s	0.42	1.19	1.09	0.98	0.58	0.92	0.97	1.26	1.60	0.93

Table A2. FFR values for various heart rates.

Patient	Stenosis	60 bpm	80 bpm	100 bpm	120 bpm
1	LAD	0.895	0.887	0.882	0.885
2	LAD	0.859	0.852	0.852	0.837
3	RCA	0.888	0.881	0.879	0.878
4	LAD	0.824	0.816	0.809	0.809
5	LAD	0.810	0.795	0.787	0.791
6	LADp	0.912	0.910	0.910	0.907
6	LADd	0.810	0.803	0.802	0.801
6	DA	0.806	0.804	0.803	0.798
7	LAD	0.630	0.624	0.612	0.618
7	LCX	0.810	0.808	0.803	0.806
8	LAD	0.915	0.913	0.910	0.911
8	LCX	0.959	0.958	0.955	0.956
9	LAD	0.889	0.888	0.885	0.883
10	LAD	0.750	0.731	0.725	0.722

Table A3. CFR values for various heart rates.

Patient	Stenosis	60 bpm	80 bpm	100 bpm	120 bpm
1	LAD	2.732	2.725	2.722	2.733
2	LAD	2.383	2.399	2.387	2.406
3	RCA	2.598	2.581	2.571	2.571
4	LAD	2.190	2.167	2.168	2.158
5	LAD	2.281	2.284	2.285	2.282
6	LADp	2.413	2.410	2.411	2.317
6	LADd	2.405	2.394	2.400	2.379
6	DA	2.538	2.523	2.512	2.514
7	LAD	1.997	1.972	1.953	1.995
7	LCX	2.365	2.365	2.366	2.411
8	LAD	2.727	2.723	2.732	2.712
8	LCX	2.861	2.860	2.864	2.848
9	LAD	2.648	2.648	2.633	2.679
10	LAD	2.344	2.325	2.323	2.311

Table A4. iFR values for various heart rates.

Patient	Stenosis	60 bpm	80 bpm	100 bpm	120 bpm
1	LAD	0.958	0.958	0.959	0.959
2	LAD	0.900	0.900	0.890	0.890
3	RCA	0.929	0.923	0.922	0.921
4	LAD	0.910	0.910	0.910	0.907
5	LAD	0.940	0.940	0.941	0.942
6	LADp	0.954	0.953	0.954	0.954
6	LADd	0.947	0.946	0.948	0.947
6	DA	0.918	0.918	0.920	0.919
7	LAD	0.817	0.821	0.825	0.824
7	LCX	0.945	0.946	0.947	0.947
8	LAD	0.964	0.964	0.963	0.963
8	LCX	0.979	0.979	0.979	0.979
9	LAD	0.966	0.971	0.967	0.987
10	LAD	0.890	0.890	0.893	0.891

References

- Gould, K.L.; Kirkeeide, R.L.; Buchi, M. Coronary flow reserve as a physiologic measure of stenosis severity. *J. Am. Coll. Cardiol.* **1990**, *15*, 459–474. [[CrossRef](#)]
- Götberg, M.; Christiansen, E.H.; Gudmundsdottir, I.J.; Sandhall, L.; Danielewicz, M.; Jakobsen, L.; Olsson, S.E.; Öhagen, P.; Olsson, H.; Omerovic, E.; et al. Instantaneous wave-free ratio versus fractional flow reserve to guide PCI. *N. Engl. J. Med.* **2019**, *376*, 1813–1823. [[CrossRef](#)]
- Gognieva, D.; Mitina, Y.; Gamilov, T.; Pryamonosov, R.; Vasilevskii, Y.; Simakov, S.; Liang, F.; Ternovoy, S.; Serova, N.; Tebenkova, E.; et al. Noninvasive assessment of the fractional flow reserve with the CT FFRc 1D method: Final results of a pilot study. *Glob. Heart* **2020**, *16*, 837.
- Gognieva, D.G.; Gamilov, T.M.; Pryamonosov, R.A.; Vasilevsky, Y.V.; Simakov, S.S.; Liang, F.; Ternovoy, S.K.; Serova, N.S.; Tebenkova, E.S.; Sinityn, E.A.; et al. Noninvasive assessment of the fractional reserve of coronary blood flow with a one-dimensional mathematical model. Preliminary results of the pilot study. *Russ. J. Cardiol.* **2019**, *24*, 60–68.
- Zheng, D.; Chen, W.; Hao, G.; Yang, X.; Luo, X.; Nicholas, A.H. A One-Dimensional Hemodynamic Model of the Coronary Arterial Tree. *Front. Physiol.* **2019**, *10*, 853. [[CrossRef](#)]
- Mynard, J.P.; Penny, D.J.; Smolich, J.J. Scalability and in vivo validation of a multiscale numerical model of the left coronary circulation. *Am. J. Physiol. Heart Circ.* **2014**, *306*, H517–H528. [[CrossRef](#)]
- Kamangar, S.; Badruddin, I.A.; Govindaraju, K.; Nik-Ghazali, N.; Badarudin, A.; Viswanathan, G.N.; Ahmed, N.; Khan, T. Patient-specific 3D hemodynamics modelling of left coronary artery under hyperemic conditions. *Med. Biol. Eng. Comput.* **2017**, *55*, 1451–1461. [[CrossRef](#)]
- Lu, M.T.; Ferencik, M.; Roberts, R.S.; Lee, K.L.; Ivanov, A.; Adami, E.; Mark, D.B.; Jaffer, F.A.; Leipsic, J.A.; Douglas, P.S.; et al. Noninvasive FFR Derived From Coronary CT Angiography: Management and Outcomes in the PROMISE Trial. *JACC Cardiovasc. Imaging* **2017**, *10*, 1350–1358. [[CrossRef](#)] [[PubMed](#)]
- Blanco, P.J.; Bulant, C.A.; Müller, L.O.; Maso Talou, G.D.; Guedes Bezerra, C.; Lemos, P.A.; Feijóo, R.A. Comparison of 1D and 3D Models for the Estimation of Fractional Flow Reserve. *Sci. Rep.* **2018**, *8*, 17275. [[CrossRef](#)] [[PubMed](#)]
- Gognieva, D.G.; Pershina, E.S.; Mitina, Y.O.; Gamilov, T.M.; Pryamonosov, R.A.; Gogiberidze, N.A.; Rozhkov, A.N.; Vasilevsky, Y.V.; Simakov, S.S.; Liang, F.; et al. Non-invasive fractional flow reserve: A comparison of one-dimensional and three-dimensional mathematical modeling effectiveness *Cardiovasc. Ther. Prev.* **2020**, *19*, 12–18. [[CrossRef](#)]
- Boileau, E.; Nithiarasu, P. One-dimensional modelling of the coronary circulation. Application to noninvasive quantification of fractional flow reserve (FFR). *Lect. Notes Comput. Vis. Biomech.* **2015**, *21*, 137–155.
- Carson, J.M.; Roobottom, C.; Alcock, R.; Nithiarasu, P. Computational instantaneous wave-free ratio (IFR) for patient-specific coronary artery stenoses using 1D network models. *Int. J. Numer. Methods Biomed. Eng.* **2019**, *35*, e3255. [[CrossRef](#)] [[PubMed](#)]
- Lee, K.E.; Kim, G.T.; Jung, E.C.; Shin, E.S.; Shim, E.B. Diagnostic performance of a vessel-length-based method to compute the instantaneous wave-free ratio in coronary arteries. *Sci. Rep.* **2020**, *10*, 1132. [[CrossRef](#)] [[PubMed](#)]
- Ge, X.; Liu, Y.; Tu, S.; Simakov, S.; Vassilevski, Y.; Liang, F. Model-based analysis of the sensitivities and diagnostic implications of FFR and CFR under various pathological conditions. *Int. J. Numer. Methods Biomed. Eng.* **2019**, e3257. [[CrossRef](#)]
- Shalman, E.; Rosenfeld, M.; Dgany, E.; Einav, S. Evaluation of CFR and FFR parameters by CFD modeling of the flow in a stenosed coronary artery. In Proceedings of the First Joint BMES/EMBS Conference, 1999 IEEE Engineering in Medicine and Biology 21st Annual Conference and the 1999 Annual Fall Meeting of the Biomedical Engineering Society, Atlanta, GA, USA, 13–16 October 1999; Volume 1, p. 217. [[CrossRef](#)]

16. Carson, J.M.; Pant, S.; Roobottom, C.; Alcock, R.; Blanco, P.J.; Carlos Bulant, C.A.; Vassilevski, Y.; Simakov, S.; Gamilov, T.; Pryamonosov, R.; et al. Non-invasive coronary CT angiography-derived fractional flow reserve: A benchmark study comparing the diagnostic performance of four different computational methodologies. *Int. J. Numer. Methods Biomed. Eng.* **2019**, *35*, e3235. [[CrossRef](#)]
17. Ge, X.; Liu, Y.; Yin, Z.; Tu, S.; Fan, Y.; Vassilevski, Y.; Simakov, S.; Liang, F. Comparison of instantaneous wave-free ratio (iFR) and fractional flow reserve (FFR) with respect to their sensitivities to cardiovascular factors: A computational model-based study. *J. Interv. Cardiol.* **2020**, *2020*, 4094121. [[CrossRef](#)]
18. Boileau, E.; Pant, S.; Roobottom, C.; Sazonov, I.; Deng, J.; Xie, X.; Nithiarasu, P. Estimating the accuracy of a reduced-order model for the calculation of fractional flow reserve (FFR). *Int. J. Numer. Methods Biomed. Eng.* **2017**, *34*, e2908. [[CrossRef](#)]
19. Waltz, J.; Kocher, M.; Kahn, J.; Leddy, R.; Chamberlin, J.H.; Cook, D.; Burt, J.R. Improving CT-Derived Fractional Flow Reserve Analysis: A Quality Improvement Initiative. *Cureus* **2020**, *12*, e10835. [[CrossRef](#)]
20. Gamilov, T.; Kopylov, P.; Serova, M.; Syunyaev, R.; Pikunov, A.; Belova, S.; Liang, F.; Alastruey, J.; Simakov, S. Computational analysis of coronary blood flow: The role of asynchronous pacing and arrhythmias. *Mathematics* **2020**, *8*, 1205. [[CrossRef](#)]
21. Vassilevski, Y.; Olshanskii, M.; Simakov, S.; Kolobov, A.; Danilov, A. *Personalized Computational Haemodynamics: Models, Methods, and Applications for Vascular Surgery and Antitumor Therapy*; Academic Press: Cambridge, MA, USA, 2020; doi:10.1016/C2017-0-02421-7. [[CrossRef](#)]
22. Simakov, S. Spatially averaged haemodynamic models for different parts of cardiovascular system. *Russ. J. Numer. Anal. Math. Model.* **2020**, *35*, 285–294.
23. Gamilov, T.; Simakov, S. Blood flow under mechanical stimulations. *Adv. Intell. Syst. Comput.* **2020**, *1028 AISC*, 143–150.
24. Barret, K.; Brooks, H.; Boitano, S.; Barman, S. *Ganong's Review of Medical Physiology*, 23th ed.; The McGraw-Hill: New York, NY, USA, 2010.
25. Noble, M.I.M.; Trenchard, D.; Guz, A. Effect of changing heart rate on cardiovascular function in the conscious dog. *Circ. Res.* **1966**, *19*, 206–213. [[CrossRef](#)]
26. Kenny, J.; Plappert, T.; Doubilet, P.; Salzman, D.; Sutton, M.G. Effects of heart rate on ventricular size, stroke volume, and output in the normal human fetus: A prospective Doppler echocardiographic study. *Circulation* **1987**, *76*, 52–58. [[CrossRef](#)] [[PubMed](#)]
27. Magomedov, K.M.; Kholodov, A.S. *Grid-Characteristic Numerical Methods*; Urite: Moscow, Russia, 2018.
28. Van de Vosse, F.N.; Stergiopoulos, N. Pulse wave propagation in the arterial tree. *Annu. Rev. Fluid Mech.* **2011**, *43*, 467–499. [[CrossRef](#)]
29. Collis, T.; Devereux, R.B.; Roman, M.J.; De Simone, G.; Yeh, J.; Howard, B.V.; Fabsitz, R.R.; Welty, T.K. Relations of stroke volume and cardiac output to body composition: The strong heart study. *Circulation* **2001**, *103*, 820–825. [[CrossRef](#)]
30. Sakamoto, S.; Takahashi, S.; Coskun, A.U.; Papafaklis, M.I.; Takahashi, A.; Saito, S.; Stone, P.H.; Feldman, C.L. Relation of distribution of coronary blood flow volume to coronary artery dominance. *Am. J. Cardiol.* **2013**, *111*, 1420–1424. [[CrossRef](#)]
31. Xaplanteris, P.; Fournier, S.; Keulards, D.C.J.; Adedj, J.; Ciccarelli, G.; Milkas, A.; Pellicano, M.; van't Veer, M.; Barbato, E.; Pijls, N.H.J.; et al. Catheter-Based Measurements of Absolute Coronary Blood Flow and Microvascular Resistance. *Circ. Cardiovasc. Interv.* **2018**, *11*, e006194. [[CrossRef](#)] [[PubMed](#)]
32. Van der Giessen, A.G.; Groen, H.C.; Doriot, P.A.; De Feyter, P.J.; Van der Steen, A.F.; Van de Vosse, F.N.; Wentzel, J.J.; Gijssen, F.J. The influence of boundary conditions on wall shear stress distribution in patients specific coronary trees. *J. Biomech.* **2011**, *44*, 1089–1095. [[CrossRef](#)] [[PubMed](#)]
33. Bulant, C.A.; Blanco, P.J.; Maso Talou, G.D.; Guedes Bezerra, C.; Lemos, P.A.; Feijóo, R.A. A head-to-head comparison between CT- and IVUS-derived coronary blood flow models. *J. Biomech.* **2017**, *51*, 65–76. [[CrossRef](#)]
34. Lo, E.W.C.; Menezes, L.J.; Torii, R. On outflow boundary conditions for CT-based computation of FFR: Examination using PET images. *Med. Eng. Phys.* **2020**, *76*, 79–87. [[CrossRef](#)]
35. Sen, S.; Escaned, J.; Malik, I.S.; Mikhail, G.W.; Foale, R.A.; Mila, R.; Tarkin, J.; Petraco, R.; Broyd, C.; Jabbour, R.; et al. Development and validation of a new adenosine-independent index of stenosis severity from coronary wave-intensity analysis: Results of the ADVISE (ADenosine Vasodilator Independent Stenosis Evaluation) study. *J. Am. Coll. Cardiol.* **2012**, *59*, 1392–1402. [[CrossRef](#)] [[PubMed](#)]
36. Gamilov, T.M.; Kopylov, P.Y.; Pryamonosov, R.A.; Simakov, S.S. Virtual fractional flow reserve assessment in patient-specific coronary networks by 1d haemodynamic model. *Russ. J. Numer. Anal. Math. Model.* **2015**, *30*, 269–276. [[CrossRef](#)]
37. Kwasiborski, P.J.; Czerwiński, W.; Kowalczyk, P.; Buksińska-Lisik, M.; Horszczaruk, G.; Aboodi, M.S.; Derbisz, K.; Hochul, M.; Janas, A.; Cwetsch, A.; et al. Influence of heart rate on FFR measurements: An experimental and clinical validation study. *Int. J. Cardiol.* **2020**, *317*, 13–17. [[CrossRef](#)]
38. Müller, L.O.; Fossan, F.E.; Bråten, A.T.; Jørgensen, A.; Wiseth, R.; Hellevik, L.R. Impact of baseline coronary flow and its distribution on fractional flow reserve prediction. *Int. J. Numer. Methods Biomed. Eng.* **2019**, e3246. [[CrossRef](#)]
39. Rossen, J.D.; Winniford, M.D. Effect of increases in heart rate and arterial pressure on coronary flow reserve in humans. *J. Am. Coll. Cardiol.* **1993**, *21*, 343–348. [[CrossRef](#)]

-
40. Alastruey, J.; Khir, A.W.; Matthys, K.S.; Segers, P.; Sherwin, S.J.; Verdonck, P.R.; Parker, K.H.; Peiró, J. Pulse wave propagation in a model human arterial network: Assessment of 1-D visco-elastic simulations against in vitro measurements. *J. Biomech.* **2011**, *44*, 2250–2258. [[CrossRef](#)] [[PubMed](#)]
 41. Xiao, N.; Alastruey-Armon, J.; Figueroa, C.A. A systematic comparison between 1D and 3D hemodynamics in compliant arterial models. *Int. J. Numer. Methods Biomed. Eng.* **2014**, *30*, 204–231. [[CrossRef](#)]